International Journal of Automotive Technology, Vol. 9, No. 6, pp. 649–657 (2008)
DOI 10.1007/s12239–008–0077–7

1229–9138/2008/043–02

EFFECT OF INTAKE VALVE SWIRL ON FUEL-GAS MIXING AND SUBSEQUENT COMBUSTION IN A CAI ENGINE

J. N. KIM[1)], H. Y. KIM[2)*], S. S. YOON[2)] and S. D. SA[1)]

[1)]Graduate School of Mechanical Engineering, Korea University, Seoul 136-701, Korea
[2)]Department of Mechanical Engineering, Korea University, Seoul 136-701, Korea

(Received 31 December 2007; Revised 8 July 2008)

ABSTRACT–A fully three-dimensional model was used to investigate the optimal value for intake valve lift in a CAI engine. Uniform mixing in the engine is a key parameter that affects the auto-ignition reliability and thermal efficiency. The method of intake of the air supply often determines the uniformity (or quality) of the fuel-air mixture. In this paper, four strategies were applied for controlling the swirl intensity of intake air. The variation of the intake valve lift induces different swirling and tumbling intensities. Both experimental data and 1D WAVE software (*Ricardo*, Co.) were coupled with the 3D model to provide pressure and temperature boundary conditions. The initial condition of the EGR mass fraction was also provided by the 1D model. The benchmark scenario (Case 1) was considered as a valve lift with 2 mm for all intake valves. We found that an intake valve lift of 6 mm with the other intake valve closed (i.e., Case 5) yielded the largest swirling (helical motion in the axial direction) and tumbling, which in turn rendered optimal fuel-gas mixing. We also found that fuel distribution affected the auto-ignition sites (or spot). The better the mixing, the greater the gas temperature and combustion efficiency achieved, as seen in Case 5. The NOx level, however, was increased due to the gas temperature. The optimal operating condition is selected from the viewpoints of environmental protection and combustion efficiency.

KEY WORDS : CAI (Controlled Auto-Ignition), NVO (Negative Valve Overlap), IEGR (Internal Exhaust Gas Recirculation), Swirl ratio

1. INTRODUCTION

The internal combustion (IC) engine continues to serve as one of the most widely used chemical energy conversion devices, particularly in the automobile industry. Because of growing public concern regarding environmental pollution, the demand for cleaner IC engines that produce lesser amounts of hazardous gases is also growing. At the same time, achieving higher thermal efficiency is equally important for reduction of the fuel consumption rate. Because of the irreconcilable tendency for increasing emissions with increases in thermal efficiency, satisfying the two requirements simultaneously, i.e., achieving higher thermal efficiency while reducing emission, has never been an easy task. For this reason, one has always had to find a compromise condition at which both requirements are never completely satisfied. However, at present, a new strategic vision needs to be outlined.

Out of many types of engine technologies, a CAI (Controlled Auto Ignition) engine using low temperature premixed combustion has been known to simultaneously reduce both environmentally hazardous emissions and the fuel consumption rate.

CAI combustion, achieved by direct injection inside a combustion dome with four valves, is generally controlled by changing the negative valve overlap (NVO) timing. Rising temperature due to cyclic compression auto-ignites the vaporized fuel within the CAI engine. Furthermore, auto-ignition is assisted by internal exhaust gas recirculation (IEGR), a mechanism used to trap high temperature exhaust residuals.

In general, premixed combustion can be categorized as "fully" and "partially" premixed combustion. In the fully premixed combustion, fuel is injected at the intake-port and is mixed well with air prior to residence inside the combustor, i.e., spark ignition engines. Direct fuel injection refers to the method by which fuel and air are first mixed inside a combustor, permitting a relatively shorter mixing period; this method is known as partially premixed combustion. In general, the CAI engine takes advantage of partially premixed combustion in an attempt to reduce the fuel consumption rate (Sjoberg *et al*., 2002). The lean F/A (fuel-air ratio) operation further offers a combustion scenario less susceptible to knocking by means of alleviating locally high temperature.

However, complex valve train systems, the difficulties associated with controlling auto-ignition time (or instance), and the energy release rate are known shortcomings of the CAI engine. These shortcomings were circumvented by intake charge heating (Oakley *et al*., 2001), compression

**Corresponding author*: e-mail: kimhy@korea.ac.kr

ratio increase (Christensen *et al*., 1999), and fuel reforming (Olsson and Johansson, 2001). However, these aforementioned remedies are impractical because their implementation necessitates an extraneous system and is limited by the small CAI operation range, reduced volumetric efficiency, and large thermal inertia.

Another alternative remedy includes the use of residual gases obtained by early closure of the exhaust valves (Li *et al*., 2001) in four-stroke engines. Kim *et al*. (2007) investigated the effect of internal EGR on the pressure, temperature, and homogeneity inside the cylinder using various exhaust valve timings. Their parametric studies showed that the peak pressure and temperature toward the end of compression stroke was decreased when the EVC timing was retarded, a behavior which may pose a danger to the engine auto-ignition due to low temperature of mixture gases. Generally, for temperatures less than 1000 K, the fuel-air mixture cannot easily be auto-ignited (Cao *et al*., 2006).

According to the Arrhenius equation (Kuo, 1986), three primary factors influencing overall combustion are temperature of mixture gas, concentration of fuel and oxidizer, and components of other co-existing species. The Arrhenius formulation implicitly indicates that the influence of temperature is relatively minor. While optimization of the chemical kinetics rate by changing gas temperature is ineffective, its control by manipulating gas mole fraction and species is more expedient. Thus, this manipulation is a viable way to control the ignition timing and subsequent combustion of the CAI engine.

Physical forcing, such as swirl originated from the intake valves, does expedite the fuel mixing process. This increased mixing rate is known to reduce smoke emissions and soot formation. The in-cylinder flow pattern is set up by the intake valve process, and the mass concentration is substantially modified during the compression processes.

The purpose of this study is to numerically examine the effects of intake port swirl on the overall performance of the CAI engine. The optimal operating condition is found by changing the intake valve lift, which comprises the main parametric studies herein.

A recommendation for the optimal operating condition is made by weighting the importance of the thermal efficiency and emission level of each computational run.

2. NUMERICAL SIMULATION DETAIL

All numerical simulations were conducted using 3D unsteady RANS (Reynolds-Averaged Navier-Stokes), a turbulent Eulerian-Lagrangian particle tracking model (Bracco, 1985). A total of three revolutions (1080 crank angle) of the piston's cyclic motion in the CAI engine was simulated. This simulation included momentum and energy transfer processes between gas and liquid fuel. The amount of internal EGR remaining after combustion inside the engine was estimated by the 1D model, called WAVE (*Ricardo*, Co.). Experimental data for pressure and temperature was provided with other necessary initial and boundary conditions for the fully 3D computation.

2.1. Governing Equation

The conservation equations for the gas phase can be described by Equation (1) with the variables given in Table 1.

$$\frac{\partial}{\partial t}(\rho\varphi)+\frac{\partial}{\partial x_j}(\rho u_j\varphi)=\frac{\partial}{\partial x_j}\left(\Gamma_\varphi\frac{\partial\varphi}{\partial x_j}\right)+S_\varphi \tag{1}$$

When liquid fuel is injected, the droplet velocity and displacement, u_{di} and x_{di}, can be expressed by

$$m_d\frac{du_{di}}{dt}=\frac{1}{2}C_D\rho A_d|u_i-u_{di}|(u_i-u_{di})-V_d\nabla p \tag{2}$$

with Newton's 2nd law of motion as below:

$$\frac{dx_{di}}{dt}=u_{di} \tag{3}$$

Table 1. Generalized equation.

	Equation	φ	Γ_φ	S_φ
Continuous phase	Continuity	1	0	$S_{d,m}$
	Momentum	u_i	μ_e	$-\frac{\partial}{\partial x_i}\left(p+\frac{2}{3}\rho k+\mu_e\frac{\partial u_k}{\partial x_k}\right)+S_{u_i}+S_{d,u_i}$
	Turbulent kinetic energy	k	$\mu+\frac{\mu_t}{\sigma_k}$	$G_k-\rho\varepsilon$
	Dissipation rate	ε	$\mu+\frac{\mu_t}{\sigma_\varepsilon}$	$\frac{\varepsilon}{k}(c_1G_k-c_2\rho\varepsilon)$
	Species	Y_s	$\frac{\lambda}{C_p}+\frac{\mu_t}{\sigma_Y}$	$S_{d,j}$
	Energy	h	$\frac{\lambda}{C_p}+\frac{\mu_t}{\sigma_h}$	$S_{d,h}$

where, $G_k=\mu_t\left(\frac{\partial u_i}{\partial x_j}+\frac{\partial u_j}{\partial x_i}\right)\frac{\partial u_i}{\partial x_j}$, $\mu_e=\mu+\mu_t$, $\mu_t=\rho c\frac{k^2}{\varepsilon}$ and σ_φ: Turb. Prantle No.

where the drag coefficient, C_D, is estimated by the correlation of Yuen and Chen (1976).

The heat and mass transfer of a single droplet are calculated using the conservation of mass and energy:

$$\frac{dm_d}{dt} = -A_s K_g p_t \ln\frac{(p_t - p_{v,\infty})}{(p_t - p_{v,s})} \tag{4}$$

$$m_d \frac{d(c_{p,d} T_d)}{dt} = -A_s h (T_d - T) + h_{fg} \frac{dm_d}{dt} \tag{5}$$

Here, K_g and h represent the mass and heat transfer coefficients, respectively, which can be obtained from the Ranz-Marshall relation (Ranz and Marshall, 1952).

As for the atomization model, the primary and secondary atomization model of Reitz and Diwakar (Reitz *et al.*, 1986) were utilized.

The auto-ignition approach is based on the shell-model (Halstead *et al*., 1977). The model uses a simplified multi-step reaction mechanism to predict the spontaneous auto-ignition of hydrocarbon fuels. Table 2 shows the reactions. *RH* is a hydrocarbon, *B* is a degenerating branching agent, *Q* represents a labile intermediate species, and *P* represents oxidized products, whose fixed proportions are determined by the molar equilibrium of CO, CO_2, and H_2O. The reaction rate constants are of the Arrhenius type:

$$f_i = A_{fi} \exp(-E_{fi}/RT) \quad \text{for } i = 2 \tag{6}$$

$$f_i = A_{fi} \exp(-E_{fi}/RT)\,[O_2]^{X_i}[RH]^{\gamma_i} \quad \text{for } i \neq 2 \tag{7}$$

where the figures in brackets refer to the mass fraction of a species.

In the combustion model, the Magnussen and Hjertager (1981) eddy breakup was used. The fuel consumption rate is given by:

$$R_F = -\frac{\rho\varepsilon}{k} A_{ebu} \min\left[Y_F, \frac{Y_o}{s_o}, B_{ebu}\frac{Y_P}{s_P}\right] \text{ kg/m}^3\text{s} \tag{8}$$

$$s_O \equiv n_O M_O / n_F M_F \tag{9}$$

$$s_P \equiv n_P M_P / n_F M_F \tag{10}$$

where *F* and *P* denote reactants and products. A_{ebu}, B_{ebu} are dimensionless empirical coefficients with values 4 and 0.5, respectively. M_m is the molecular weight and n_m is stoichiometric coefficient (i.e., number of moles).

Table 2. Shell model reactions.

Reaction number	Reactants	Equilibrium constant	Product	Reaction type
1	$RH+O_2$	K_q	$2R^*$	Initiation
2	R^*	K_p	R^*+P+Heat	Propagate
3	R^*	f_1K_P	R^*+B	Form *B*
4	R^*	f_4K_P	R^*+Q	Form *Q*
5	R^*+Q	f_2K_P	R^*+B	Form *B*
6	*B*	K_b	$2R^*$	Degenerate
7	R^*	f_3K_P	Out	Terminate
8	$2R^*$	K_t	Out	Terminate

2.2. Grid Generation

The basic test engine is a single cylinder, four-stroke gasoline direct injection engine, used frequently for CAI research, with the following dimensions: bore diameter - 88 mm, stroke length - 97 mm, connecting rod length - 143.75 mm, and compression ratio - 10.5:1.

For the gas exchange processes, a moving-grid was created from the CAD geometry and surface mesh using ES-ICE, which is a grid-generation tool used to facilitate moving-grid transient analyses of internal combustion in the CAI engine. Figure 1 shows the CAD geometry and the constructed grid for the CAI engine used in the current study. The number of cells basically depends on both the instantaneous valve lift and the position of the piston. When the piston is at the TDC (Top Dead Center) position, the grid resolution begins with approximately 213,000 nodes and increases up to about 518,000 nodes at the BDC (Bottom Dead Center) position.

2.3. Numerical Schemes and Parametric Studies

The 3D full-cycle simulations were performed using the software STAR-CD (*CD-Adapco*). STAR-CD is a finite volume-based code, which incorporates and solves the compressible form of the Navier-Stokes equations. To solve the flow field, a fully-implicit scheme is used for temporal discretization. Thus, the Monotone Advection and Reconstruction Scheme (Asproulis, 1994) is used for

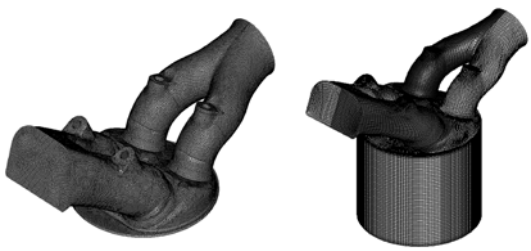

(a) CAD geometry (b) Constructed grid

Figure 1. CAD geometry and generated grid.

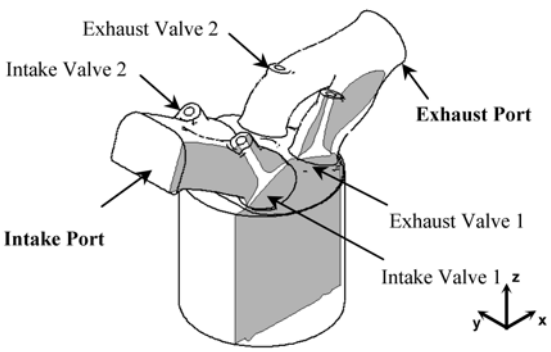

Figure 2. Single cylinder engine schematic for CAI research.

Table 3. Operating conditions for intake valve lift strategy.

	Valve lift (mm)				
Valve	Case 1	Case 2	Case 3	Case 4	Case 5
Intake valve (IV) 1	2	2	2	0	0
Intake valve (IV) 2	2	4	6	4	6

the differencing process, and the PISO-algorithm (Issa, 1986) is used for time integration.

Figure 2 shows the schematic of the CAI engine and Table 3 lists a total of five cases considered in the current parametric studies. Case 1 is the benchmark scenario, with a valve lift of 2 mm for both intake valves.

In all cases, the valve timings (EVO/EVC and IVO/IVC) have constant values (140/290 and 440/590 CAD ATDC) according to the temperature of the NVO period. The maximum exhaust valve lift also has a fixed value (2 mm) because an equal internal EGR quantity has to be applied to all cases.

For Cases 2 and 3, the value of IV2 (Intake Valve 2) was varied to 4 mm and 6 mm while the other IV1 (Intake Valve 1) was fixed as 2 mm. For Cases 4 and 5, IV2 was increased up to 4 mm and 6 mm, respectively, with the other intake valve closed (i.e., IV1=0).

For boundary conditions, the pressure at the intake and exhaust ports was assumed to be a constant at 1 bar, modeling a boost system implemented with a turbo-charger.

No-slip wall boundary conditions were applied to all solid surfaces. The initial temperature at every component was set as follows: cylinder wall - 400 K, piston head - 520 K, cylinder head - 520 K, and valve head - 800 K. The 3D simulation necessitated approximately 84 hours of computation for one complete cycle on a platform featuring two Intel Zeon Dempsey 3.2 GHz Processors and 8 Gbytes of RAM.

3. RESULTS AND DISCUSSION

3.1. 1D Gas Dynamics Simulation

A 1D gas dynamics engine system simulation code (*Ricardo*, WAVE) was used to provide the boundary conditions for the 3D computation.

This code handles flows through pipes, valves, and cylinders and the general thermodynamics of an engine, manifolds, and supercharger. The modeling results from the WAVE code include time dependent pressures, temperatures, and mass flows for the manifold air inlet and the intake port outlets to the cylinders.

The simulation was performed for Case 1 operating conditions with 2000 rpm. Figure 3 shows the pressure-volume diagram in the simulation results. The area α was added to the conventional cycle p-V diagram area because of the pressure increase due to the residual gas during NVO. The intake port inlet and outlet boundary conditions from 1D computations were used as the initial boundary conditions in the 3D computation. Figure 4 shows the comparison of the pressure histories obtained from the 1D and 3D models; their maximum deviation from each other is less than about 5%.

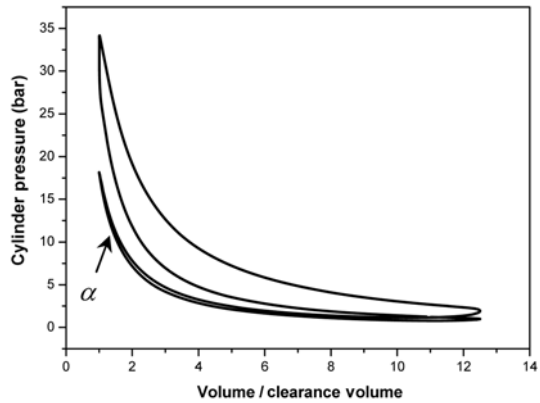

Figure 3. Pressure-volume diagram from 1D simulation results for Case 1 operating condition.

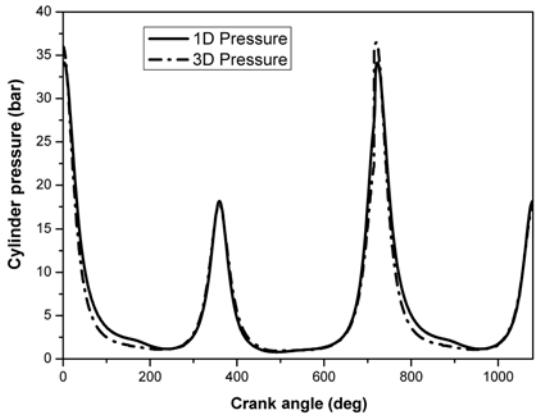

Figure 4. Cylinder pressure variation with crank angle. The simulation results were obtained for Case 1 using 1D and 3D models.

3.2. CFD 3D Simulation

3.2.1. Evaluation of the vortical motion effects

In IC-engines, there are two typical vortical motions known as "swirling" and "tumbling," which refer to the vortical motion in the x-y plane and the z-x plane (and z-y plane), respectively.

Because the valve lift profile directly influences the in-cylinder flow development during the intake process, the objective of the 3D modeling effort was to relate the valve lift profile to the flow structures. One way of representing the flow structure inside the cylinder is the use of the swirl number (or ratio), *NS*, and tumble numbers (or ratios), *NT*x, *NT*y. The equations of Mattarelli *et al*. (2004) were utilized to calculate the swirling and tumbling angular velocities. The angular velocity of the swirling motion (ω_s) is given by:

$$\omega_s = \frac{\sum_{i=1}^{n} m_i[(y_i - y_0)u_i - (x_i - x_0)v_i]}{\sum_{i=1}^{n} m_i[(x_i - x_0)^2 + (y_i - y_0)^2]} \quad (11)$$

where the number of cells within the cylinder is represented by n, the mass within each cell by m_i, the Cartesian coordinates of the local cell centroid by (x_i, y_i, z_i), the Cartesian coordinates of the cylinder axis by (x_0, y_0), and the velocity components of the local cell by (u_i, v_i, w_i).

The equations used to calculate the tumbling angular velocities (ω_{tx}, ω_{ty}) are similar to Equation (11).

$$\omega_{tx} = \frac{\sum_{i=1}^{n} m_i[(y_i - y_0)w_i - (z_i - z_0)v_i]}{\sum_{i=1}^{n} m_i[(z_i - z_0)^2 + (y_i - y_0)^2]} \quad (12)$$

$$\omega_{ty} = \frac{\sum_{i=1}^{n} m_i[(z_i - z_0)u_i - (x_i - x_0)w_i]}{\sum_{i=1}^{n} m_i[(x_i - x_0)^2 + (z_i - z_0)^2]} \quad (13)$$

Figure 5 presents the plots of the swirl numbers as a function of the crank angle during the intake stroke. The positive and negative values imply the clockwise and counter-clockwise flows, respectively. The swirl intensity increases as the valve lift increases. One noticeable behavior from Figure 5 is the strong effect of the closure of one intake port on the swirling properties of the flow. With IV1=0, as in Cases 4 and 5, the swirl intensity substantially increases at the end of the intake stroke in comparison to that of the benchmark scenario (Case 1).

Figure 6 shows x-axis tumble number histories as a function of the crank angle during the intake stroke. The x-axis tumble intensity increases as the valve lift increases but gradually loses its momentum at the end of the intake stroke. This flow behavior does not warrant enhancement of uniform mixing. Figure 7 shows y-axis tumble number histories with increase in the crank angle. The flow direction gradually changes from the clockwise to the counter-clockwise direction at the end of the intake process.

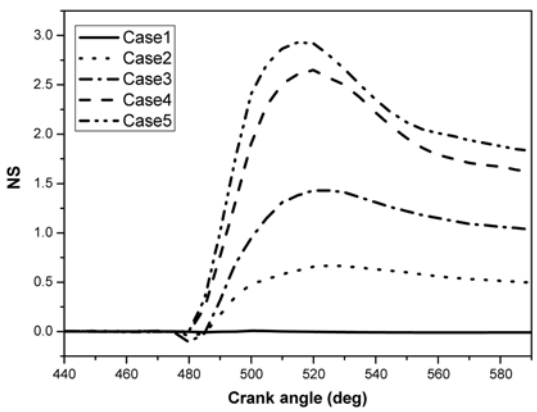

Figure 5. Swirl number variation with crank angle.

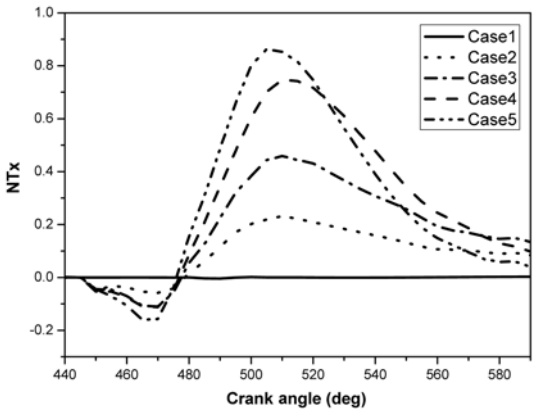

Figure 6. X-axis tumble number variation with crank angle.

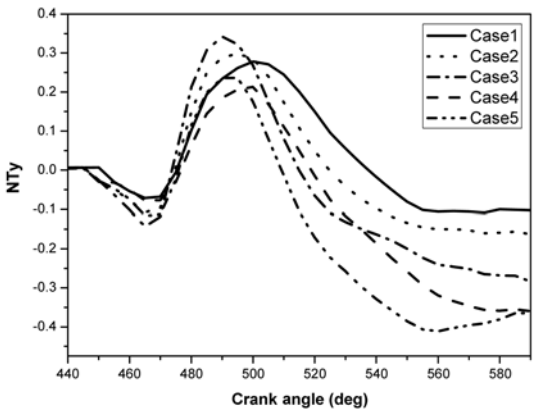

Figure 7. Y-axis tumble number variation with crank angle.

The results in Table 4 show the rotating flow numbers at the end of the intake stroke. The flow numbers of Case 5 are the highest among Cases 1~5 considered herein. *NS*, *NT*x, and *NT*y were 22.9 times, 1.3 times, and 3.7 times those of Case 1, respectively.

In order to evaluate the effects of rotating flows on fuel distribution, the uniformity index γ is calculated (Weltens *et al.*, 1993) and defined as follows:

$$\gamma = 1 - \frac{1}{2n}\sum_{i=1}^{n} \frac{\sqrt{(w_i - \bar{w})^2}}{w_i} \quad (14)$$

where w_i and $\bar{w}$ are the local and average fuel mass frac-

Table 4. Rotating flow numbers at the end of intake stroke.

	Case 1	Case 2	Case 3	Case 4	Case 5
NS	–0.08	0.50	1.03	1.61	1.83
NTx	0.03	0.08	0.13	0.10	0.04
NTy	–0.10	–0.16	–0.28	–0.36	–0.37

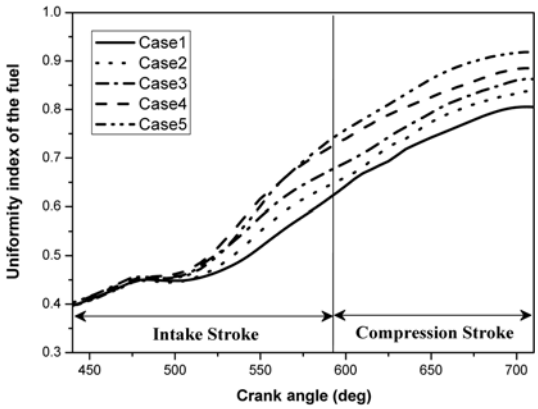

Figure 8. Fuel uniformity index for various valve lifts.

Table 5. Fuel uniformity index at 10 CAD BTDC.

Case	Uniformity index	Comparison with bench scenario (Case 1)
Case 1	0.80	N.A.
Case 2	0.84	5% Increase
Case 3	0.86	7.5% Increase
Case 4	0.89	11% Increase
Case 5	0.92	15% Increase

tions, respectively.

When γ=1, the fuel distribution is totally homogeneous, and when γ approaches zero, the fuel is completely unmixed with other gases.

Figure 8 shows the calculated uniformity index of the fuel. The index values gradually increase during the compression stroke. Table 5 shows the fuel uniformity indices and their differences from that of Case 1 at 10 CAD BTDC. The results in Table 5 show that Case 5 offered the best condition for subsequent combustion because it had the best mixing quality. The other cases show the uniformity index gain of 5%~11% over that of Case 1. This result implies that rotating flow by the difference of the intake valve lifts increases the fuel homogeneity.

Table 6. Equivalence ratio for cases 1~5.

	Case 1	Case 2	Case 3	Case 4	Case 5
Equivalence ratio	0.71	0.65	0.63	0.75	0.68

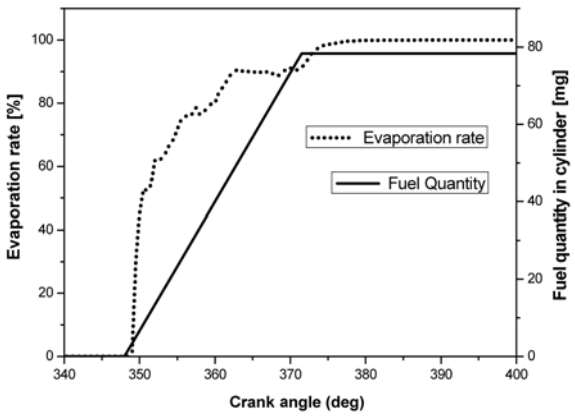

Figure 9. Fuel quantity and evaporation rate.

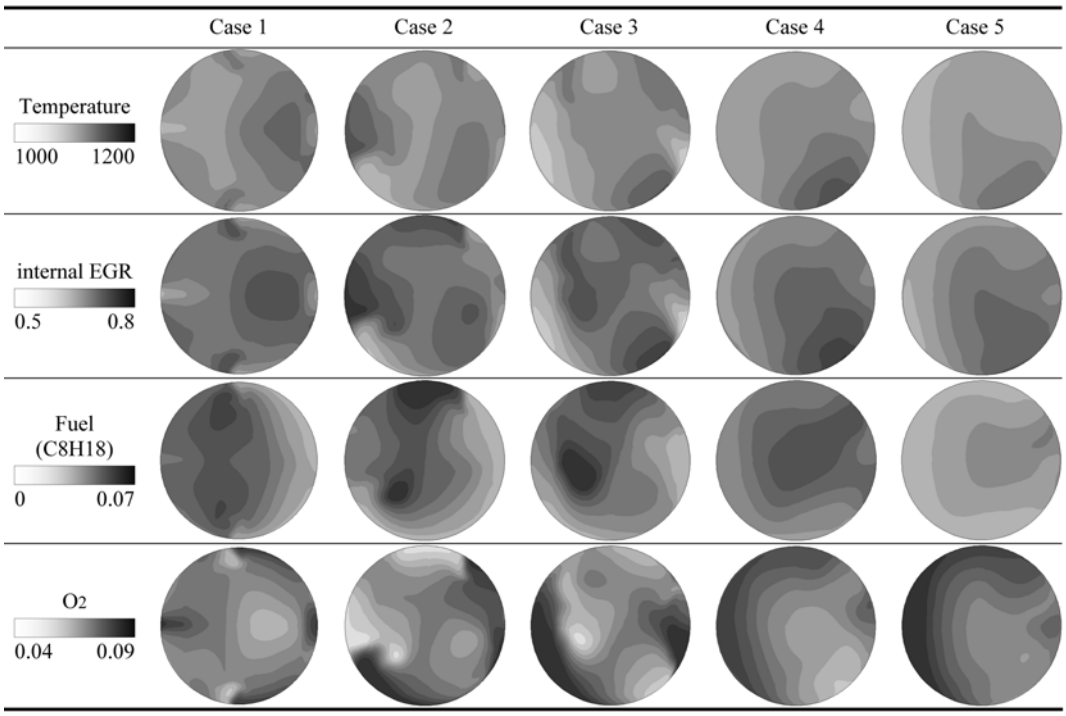

Figure 10. Temperature and mass concentration for various valve lift at 710 CAD ATDC (10 CAD BTDC).

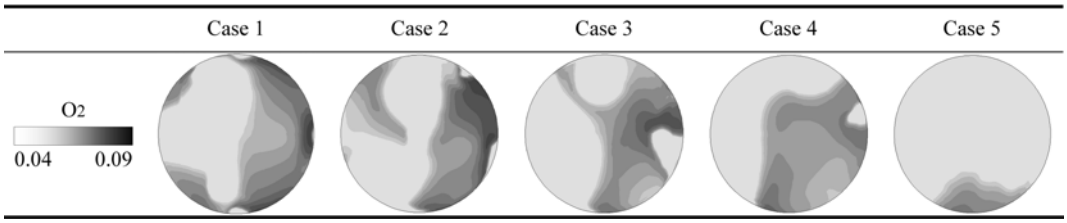

Figure 11. Oxygen concentration for various valve lift at 715 CAD ATDC (5 CAD BTDC).

3.2.2. Combustion and emission characteristics

The fuel was assumed to be iso-octane (RON 90) and was injected during the re-compression stroke (i.e., 348~372 CAD ATDC, approximately at 2 ms). Figure 9 shows the fuel quantity and evaporation rate during the re-compression stroke for Case 1. The injected fuel was quickly evaporated because of the high temperature (about 1200 K) of the internal EGR during the re-compression stroke. An evaporation rate of 100% occurred at about 388 CAD ATDC, as shown in Figure 9. The total mass of the injected fuel was set to 78.3 mg but the equivalence ratio changed due to variation of the intake valve lift, allowing a different mass flow rate of air to be induced in the combusting cylinder. As shown in Table 6, Case 4 gives a relatively richer equivalence ratio than that of other cases because of the smaller area through which the intake air was passing.

Snapshots manifesting distribution of temperature and mass fractions for all cases are shown in Figure 10; the time which the snapshots were taken was 710 CAD ATDC (10 CAD BTDC). The correlation between the temperature and local internal EGR mass fraction is shown. It is worthwhile to mention that the areas with high internal EGR mass fraction correspond to relatively high temperature areas. However, auto-ignition areas correspond to the fuel concentration as shown in Figure 10 and 11, except for Case 4. For Case 4, auto-ignition was not affected by fuel but by oxygen concentration, as indicated in Figures 10 and 11. Based on the results in Table 6, the auto-ignition behavior in Case 4 is related to the lower oxygen mass fraction.

A correlation exists between the location of high fuel concentration and the locations of auto-ignition spots in CAI engines when the fuel-air ratio is low (or lean). Thus, a larger auto-ignition spot appeared in the reaction zones for the most homogeneous mixture, as shown in Case 5.

Figure 12 and Figure 13 show histories of the cylinder pressure and temperature, respectively. For all cases, pressure and temperature rise quickly and reach their peaks at around 715 CAD ATDC (5 CAD BTDC). Among all five cases, the results from Case 5 record the highest pressure and temperature. These results imply that the homogeneous mixture improves the air usage, therefore yielding better combustion efficiency. The maximum pressure and temperature in Case 5 were about 35.7 bar and 2010 K, respectively, at 720 CAD ATDC (TDC). Though swirling was the weakest in Cases 2 and 3, the peak cylinder temperature and combustion efficiency in these cases are moderately high, and fall in the order of Case 5, 3, 2, 1, and 4, as shown in Figures 12 and 13.

The maximum pressure in Cases 2 and 3 was 33.0 and 34.1 bar, respectively, and the maximum temperature in Case 3 and 4 was 1773 and 1845 K around 720 CAD ATDC (TDC), respectively.

With respect to the highest equivalence ratio condition among all cases, Case 4 yielded the lowest pressure and temperature, 29.1 bar and 1543 K. Case 4 had a relatively high mixing quality, but the equivalence was richer than that of the benchmark scenario, Case 1. It is reasoned that the supplied oxygen was not sufficient for simultaneous auto-ignition.

Figure 14 shows the CO_2 mass fraction inside the cylinder.

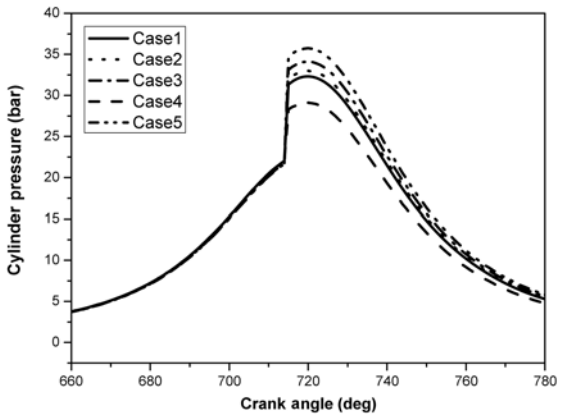

Figure 12. Predicted pressure inside the cylinder.

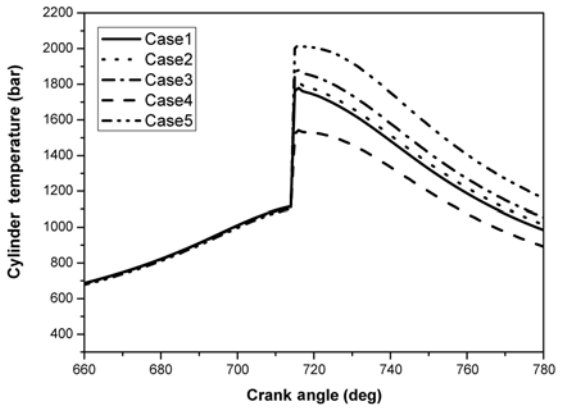

Figure 13. Predicted temperature inside the cylinder.

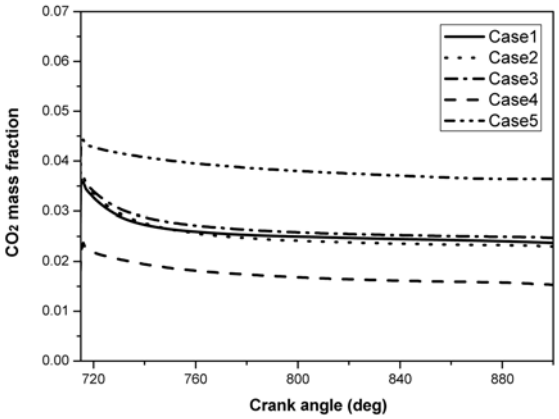

Figure 14. CO_2 mass fraction inside cylinder.

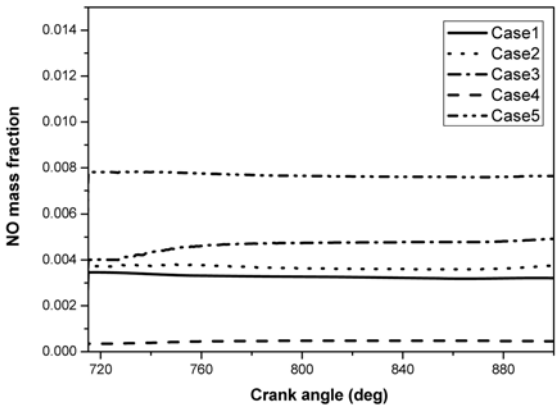

Figure 15. NO mass fraction inside cylinder.

CO_2 emissions begin to appear at the time at which the maximum temperature was recorded. The most homogeneous mixture, Case 5, retained the highest level of CO_2 because of efficient combustion. On the other hand, Case 4, in which the lowest pressure and temperature were marked, yielded the smallest amount of CO_2. The amount of CO_2 in Cases 2 and 3 were comparable to that of the benchmark Case 1.

Thermal nitric oxide formation is modeled by the Zeldovich's reaction mechanism (Zeldovich *et al*., 1947). Assuming no OH formation and a partial equilibrium state, NO formation is predicted by following global reaction, where only the forward reaction is considered:

$$N_2 + O_2 \rightarrow 2NO \quad (15)$$

Figure 15 shows the mass fraction of NO, which is maximized in the region of the highest temperature. Consequently, Case 5, yielding the highest temperature (2010 K), clearly produced the largest NO emission among all five cases. It is well known that temperature has great influence on NOx formation, especially at temperatures greater than 1800 K, according to Christensen *et al*. (1998). We too found that the NO mass fraction increased substantially when the peak temperature was greater than 1800 K (see Figure 13). The lowest peak temperature, 1543 K, was seen in Case 4, and NO formation was the smallest, as shown in Figure 15. Thus, Case 4 is the most suitable condition at which the engine can operate from the viewpoint of environmental protection.

It can be concluded that Cases 5 and 4 offer the best optimal conditions for thermal and emission efficiency, respectively. Case 3, however, seems to be the best compromise solution at which both thermal efficiency and environmental requirements are satisfied because combustion efficiency is moderately high (second order) and emission levels were comparable to that of the benchmark Case 1.

4. CONCLUSION

Uniform mixing in the engine is a key parameter that affects the auto-ignition reliability and thermal efficiency. The methods of supplying the intake air, swirling or/and tumbling, often determine the quality or uniformity of mixing. To investigate the effects of swirl on fuel-air mixing and its subsequent combustion for a CAI engine, parametric studies were conducted by using a fully three-dimensional model; the intake valve lift was varied from 0 to 6 mm. A one-dimensional model was used to provide the boundary conditions for the 3D computation. The data showed that some areas with a high internal EGR mass fraction inside the cylinder correspond to relatively high temperature areas. We also found that high fuel concentration and the auto-ignition spots affected each other, and that this effect is especially prominent when the equivalence ratio is low. Case 5, with the most homogeneous mixture, yielded the best combustion efficiency. However, the higher temperature, as in Case 5, increased the amount of nitric oxide (NO) emissions.

Therefore, in satisfying the concerns with thermal efficiency and emissions, Case 3 was considered to present the best compromised operating condition of the intake valve lift.

ACKNOWLEDGEMENT–This research was supported by a grant from Development of Engine System for HEV Project, funded by the Ministry of Commerce, Industry and Energy.

REFERENCES

Asproulis, P. N. (1994). *High Resolution Numerical Predictions of Hypersonic Flows on Unstructured Meshes.* Ph.D. Dissertation. Imperial College. England.

Bracco, F. V. (1985). Modeling of engine sprays. *SAE Paper No*. 850394.

Cao, Li., Zhao, H., Jiang, X. and Kalian, N. (2006). Investigation into the effect of injection timing on stoichiometric and lean CAI operations in a 4-stroke GDI engine. *SAE Paper No*. 2006-01-0417.

Christensen, M., Hultqvist, A. and Johansson, B. (1999).

Demonstrating the multi-fuel capability of a homogeneous charge compression ignition engine with variable compression ratio. *SAE Paper No.*1999-01-3679.

Christensen, M. and Johansson, B. (1998). Influence of mixture quality on homogeneous charge compression ignition. *SAE Paper No.* 982454.

Halstead, M., Kirsch, L. and Quinn, C. (1977). The autoignition of hydrocarbon fuels at high temperatures and pressures - Fitting a mathematical model. *Combustion and Flame,* **30**, 45–60.

Issa, R. I. (1986). Solution of the implicitly dixcretised fluid flow equations by operator-splitting. *J. Comp. Phys.*, **62**, 40-65.

Kim, J. N., Kim, H. Y., Yoon, S. S., Sa, S. D. and Kim, W. T. (2007). Effect of valve timing and lift on flow and mixing characteristics of a CAI engine. *Int. J. Automotive Technology* **8**, **6**, 687–696.

Kuo, K. K. (1986). *Principles of Combustion*. Wiley-Interscience. New York, U.S.A, 115–124.

Li, J., Zhao, H. and Ladommatos, N. (2001). Research and development of controlled auto-ignition combustion in a 4-stroke multi-cylinder gasoline engine. *SAE Paper No.* 2001-01-3608.

Magnussen, B. F. and Hjertager, B. W. (1981). On the structure of turbulence and a generalised eddy dissipation concept for chemical reaction in turbulent flow. *19th AIAA Aerospace Metting, St.Louis,* U.S.A.

Mattarelli, E., Borghi, M., Balestrazzi, D. and Fontanesi, S. (2004). The influence of swirl control strategies on the intake flow in four valve HSDI diesel engines. *SAE Paper No.* 2004-01-0112.

Oakley, A., Zhao, H., Ma, T. and Ladommatos, N. (2001). Experimental studies on controlled auto-ignition (CAI) combustion of gasoline in a 4-stroke engine. *SAE Paper No.* 2001-01-1030.

Olsson, J. and Johansson, B. (2001). Closed loop control of an HCCI engine. *SAE Paper No.* 2001-01-1031.

Ranz, W. E. and Marshall, W. R. (1952). Evaporation from drops-Part I and II. *Chem. Eng. Prog.* **48**, **3**, 141.

Reitz, R. D. and Diwakar, R. (1986). Effect of drop breakup on fuel sprays. *SAE Paper No.* 860469.

Sjoberg, M., Edling, L.-O., Eliassen, T., Magnusson, L. and Angstrom, H.-E. (2002). GDI HCCI: Effects of injection timing and air swirl of fuel stratification, combustion and emissions formation. *SAE Paper No.* 2002-01-0106.

Weltens, H., Bressler, H., Terres, F., Neumaier, H. and Rammoser, D. (1993). Optimization of catalytic converter gas flow distribution by CFD prediction. *SAE Paper No*. 930780.

Yuen, M. C. and Chen, L. W. (1976). On drag of evaporating liquid droplets. *Combust. Sci. and Tech.,* **14**, 147–154.

Zeldovich, Y. B., Sadovnikov, P. Y. and Kamenetskii, F. (1947). *Oxidation of Nitrogen in Combustion*. Institute of Chemical Physics. Moscow-Leningrad.